

REVIEW ARTICLE

Open Access

# Hierarchically engineered nanochannel systems with pore-in/on-pore structures

Minmin Li<sup>1,2</sup>, Yuchen Cao<sup>2</sup>, Yuting Xiong<sup>1,2</sup> and Guangyan Qing<sup>2</sup> 

## Abstract

Biological ion channels featuring asymmetries in structure, composition, and charge distribution have superior controllable ion transport properties, such as ion selectivity, ion gating, and ion rectification, by which life executes diverse activities, including signal transduction, cell motility, and mass and energy transfer. Inspired by this, researchers have never stopped pursuing artificial ion channels that can achieve comparable functions. Despite successful explorations in many fields, current homogeneous nanochannels, however, have not yet offered sufficient rewards comparable to those of their natural counterparts. However, hierarchically engineered heterogeneous nanochannels have gradually come onto the stage because of their excellent ion selectivity, permeability, and rectification properties and thus have been shining brilliantly in fields such as selective ion transport, energy conversion, biomolecular separation, and detection. In this article, we briefly review the recent advances of hierarchically engineered nanochannel systems in terms of pore-on-pore and pore-in-pore structures, with an emphasis on promising applications, including ion-selective transport, osmotic energy harvesting, separation, and biosensing. Finally, current challenges and conceivable solutions are also discussed to advance the design and applications of hierarchical nanochannel systems.

## Introduction

Over billions of years, biological systems have evolved into numerous elaborate structures with diverse functions. Biological ion channels, as one of Nature's wondrous works, are a type of pore-forming transmembrane protein that creates a pathway for ions to pass through the plasma membrane (Fig. 1a). These channels are generally nanoscale asymmetric in structure, composition, and charge distribution<sup>1</sup>. It is the characteristic that allows them to regulate transmembrane ion flow with high efficiency and selectivity and exhibit gated or rectified ion transport properties<sup>2</sup>, which finally contribute to various life activities, such as mass transfer, energy conversion, and signal transmission. For example, potassium ion ( $K^+$ )

channels enable rapid and selective  $K^+$  rectified transport. A structural examination reveals that pore size and critical amino acid residues are key factors of selective ion transport, which has laid a foundation for understanding the mechanisms of selective ion transport<sup>3</sup>. However, most biological ion channels with excellent ion transport properties are not fully compatible with application requirements due to inevitable limitations, such as fragile mechanical and chemical properties. Thus, understanding the fundamental characteristics and functions of biological ion channels has provided design guidelines for artificial analogs with excellent mechanical stability<sup>4</sup>. Nevertheless, it remains challenging to design and construct artificial ion channels that can perfectly execute comparable functions with their biological counterparts<sup>5</sup>.

Various artificial ion channels have been constructed to attempt to achieve rectified and selective ion transport<sup>6</sup>. To this end, one method is to mimic the key features of biological ion channels, such as exquisite structures and interfacial chemistries. In this regard, some homogeneous

Correspondence: Yuting Xiong (xiongyt@dicp.ac.cn) or Guangyan Qing (qinggy@dicp.ac.cn)

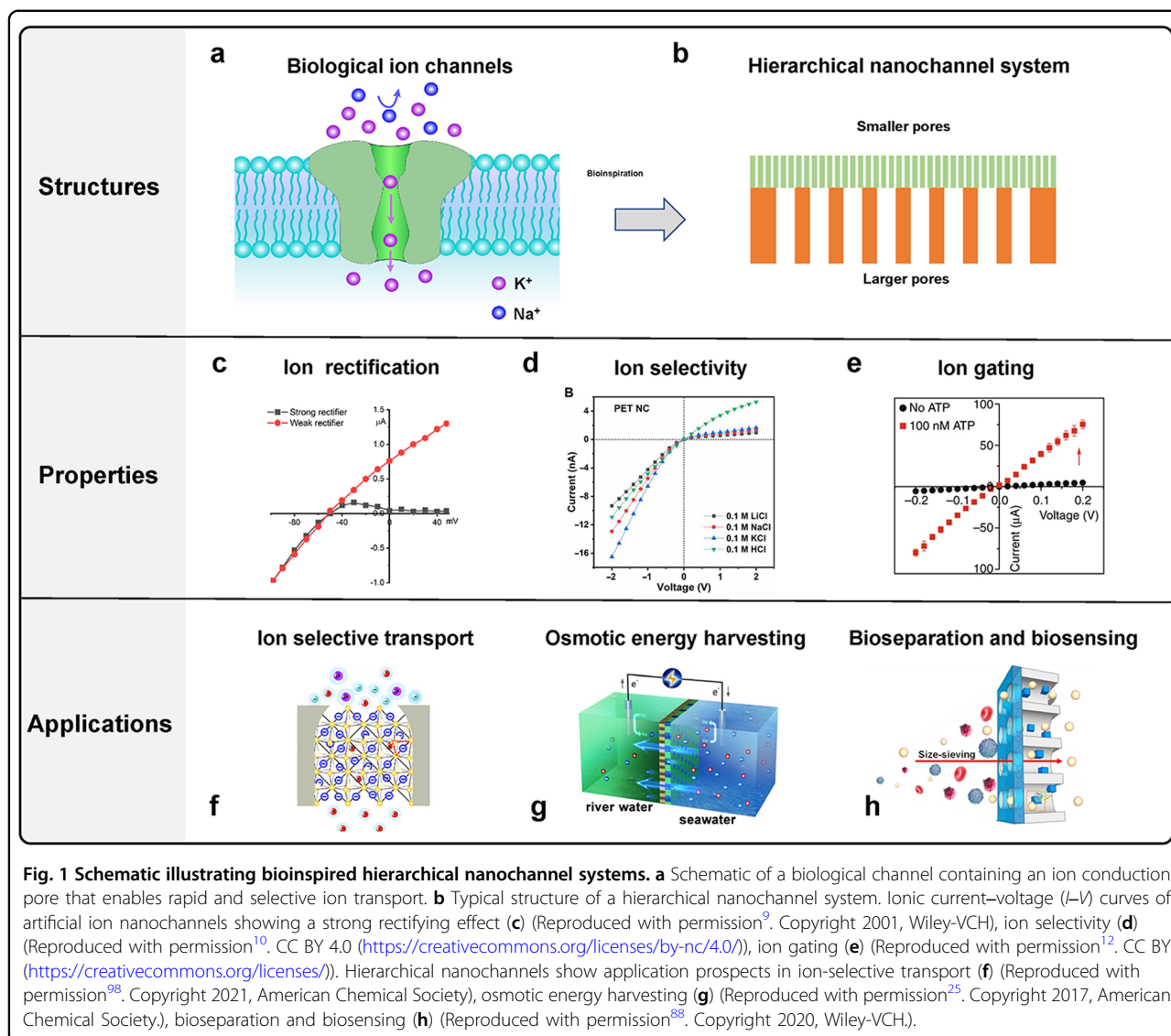
<sup>1</sup>Jiangxi Province Key Laboratory of Polymer Micro/Nano Manufacturing and Devices, East China University of Technology, Nanchang 330013, China

<sup>2</sup>CAS Key Laboratory of Separation Science for Analytical Chemistry, Dalian Institute of Chemical Physics, Chinese Academy of Sciences, Dalian 116023, China

© The Author(s) 2023



**Open Access** This article is licensed under a Creative Commons Attribution 4.0 International License, which permits use, sharing, adaptation, distribution and reproduction in any medium or format, as long as you give appropriate credit to the original author(s) and the source, provide a link to the Creative Commons license, and indicate if changes were made. The images or other third party material in this article are included in the article's Creative Commons license, unless indicated otherwise in a credit line to the material. If material is not included in the article's Creative Commons license and your intended use is not permitted by statutory regulation or exceeds the permitted use, you will need to obtain permission directly from the copyright holder. To view a copy of this license, visit <http://creativecommons.org/licenses/by/4.0/>.



nanochannel systems have achieved promising functions, such as ion transport regulation, recognition, and sensing, by taking advantage of physical and chemical modification or the construction of asymmetric nanochannel shapes<sup>7</sup>. Nevertheless, these channels have not presented sufficient rewards equal to those of their natural counterparts. Hence, hierarchically engineered nanochannel systems that were generally formed from two or more chemical compositions (Fig. 1b) have gradually come onto the stage. From a structural point of view, hierarchical nanochannels have rich and complex pore architectures from the combination of multichannels with different arrangements, structures and pore sizes<sup>8</sup>. By imitating the nanoscale asymmetric structure of biological ion channels, hierarchical nanochannels that usually possess both larger pores and smaller pores can be endowed with good ionic current rectification properties (Fig. 1c)<sup>9</sup>.

Among these, smaller pores with sizes comparable to some ions provide size sieving ability and can intensify the specific binding between ions and the channel walls, leading to an exceptional ion-selective transport property (Fig. 1d)<sup>10</sup>. From the viewpoint of interfacial properties, hierarchical nanochannels consist of various chemical compositions with different surface charges, wettability, functional groups, and chemical properties, which further strengthen the asymmetry and thus result in a more significant ionic current rectification effect. Moreover, proper chemical residues/groups that are exposed or functionalized on the inner pore walls can further improve the selectivity<sup>7,11</sup>. The introduction of some functional elements can achieve the ion gating property in response to external physical and chemical stimuli (Fig. 1e)<sup>12–14</sup>, which enables the creation of functional ion nanochannels or sensing systems.

In this review article, we summarize the advances in hierarchical nanochannel systems with two types of structures (pore-on-pore and pore-in-pore) during the past 5 years. The first section briefly introduces the design rationales. Then, we highlight the exceptionally promising applications of hierarchical nanochannels in ion-selective transport (Fig. 1f), osmotic energy harvesting (Fig. 1g), and bioseparation and biosensing (Fig. 1h). Finally, we conclude this review with our insights and perspectives on the development of this field.

### Design of hierarchical nanochannel systems

The main design rationale for hierarchical nanochannels is improving the structural and chemical selectivity of nanochannels to ions by controlling the sophisticated structures and the distribution of chemical residues on channel walls. On the one hand, hierarchical nanochannels can be precisely designed by controlling the structural parameters of different pores, such as the scale range of the pores (angstrom-scale or nanoscale), the respective ratios of small pores to large pores, the pore shape (symmetric or asymmetric geometry), the ordering degree of the pores (ordered or disordered) and others<sup>8</sup>. The existence of smaller pores makes the hierarchical nanochannel system an excellent ion-selective-transport support with regard to physical size. On the other hand, the hierarchical nanochannels are generally composed of different chemical compositions, which have the advantage of integrating the superior properties of the different materials. By arranging chemical constituents with specific charge, wettability, and chemical groups in the different parts, the selectivity of ions or molecules of the hierarchical nanochannels can be further modulated<sup>4</sup>.

The typical structures of hierarchical nanochannels with pore-in/on-pore structures are shown in Fig. 2. Pore-in-pore structures are usually fabricated by the confined growth of porous crystals in a single asymmetrical nanochannel. Porous crystals typically include metal organic frameworks (MOFs), covalent organic frameworks (COFs), porous organic salt materials, molecular crystals, etc. Diverse functional sites in their uniform angstrom-sized pores can enhance the specific binding between ions and the pore walls, making them increasingly achieve exceptional ion transport properties<sup>15–18</sup>. Taking advantage of the confined growth of porous crystal materials in nanochannels through in-situ growth<sup>19–22</sup> and seeding-facilitated interfacial growth<sup>23</sup>, an ultraselective and fast ion channel is likely to be established<sup>24</sup>. This allows the direct elucidation of the ion transport mechanism and explorations for broad electrochemical applications.

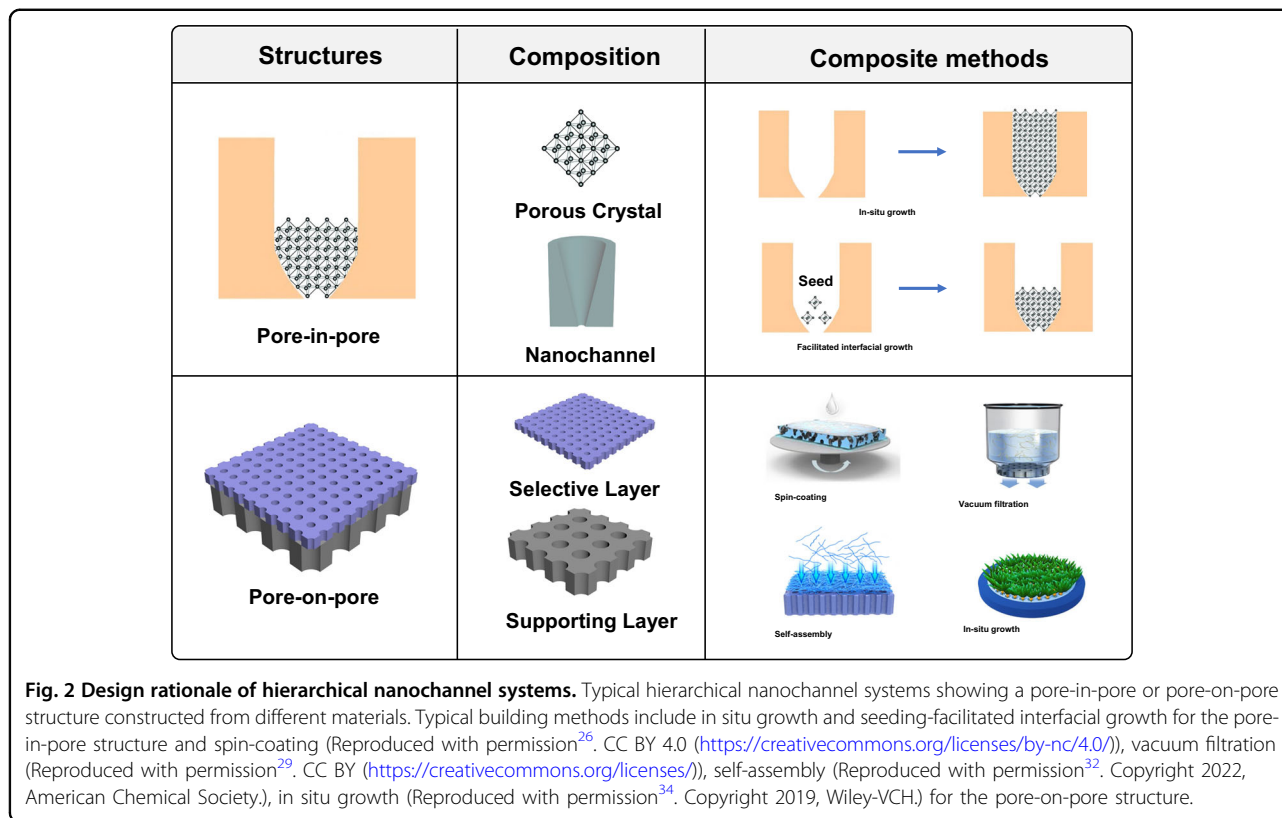
Typical hierarchically engineered nanochannel systems with pore-on-pore structures are generally formed by the hybridization of two multichannel membranes with different chemical compositions (Fig. 2). The layer with large

pores usually serves as the supporting layer, while the layer with small pores functions as the selector<sup>25,26</sup>. Hence, hierarchical nanochannels should be designed to consist of ultrasmall nanochannels, such as nanochannels constructed by random polymers and nanofibers, which can thus provide a confined space for the selective transport of ions or molecules. Accordingly, the support layer can be relatively robust and high-flux nanochannels, for example, porous anodic aluminum oxide (AAO), track-etched polyethylene terephthalate (PET) nanochannels, and self-assembled polymer membranes with rich large channels inside. The corresponding composition methods typically include spin coating<sup>25–27</sup>, vacuum filtration<sup>28,29</sup>, self-assembly<sup>30–32</sup>, in situ growing<sup>33,34</sup>, electrospinning<sup>35</sup>, etc. Overall, the obtained hierarchical nanochannel systems with excellent ion/molecule selectivity and ion rectification properties have broad application prospects in a variety of fields.

### Ion-selective transport

The natural potassium channel from *Streptomyces lividans* (the KcsA K<sup>+</sup> channel) enables rapid and selective K<sup>+</sup> transport by virtue of an asymmetric channel and a queue of binding sites (Fig. 3a). In light of this, many research groups have started researching functional recognition elements that can bind and release K<sup>+</sup> ions and have presented various artificial K<sup>+</sup> channels based on crown ethers<sup>36</sup>, cyclodextrin<sup>37</sup>, and helical oligomers<sup>38</sup>. Despite excellent K<sup>+</sup> selectivity, these chemical channels remain subject to poor robustness. Materials with intrinsic high nanoporosity as potential candidates for the use of ion transport might help to overcome this limitation. Recently, Xin et al. for the first time attempted to employ a porous crystal as the channel carrier to achieve ultraselective K<sup>+</sup> transport<sup>22</sup>. The self-assembled crystalline porous organosulfonate-amidinium salts (CPOs) have sequential channel structures similar to those of natural KcsA K<sup>+</sup> channels, as shown in Fig. 3b. When CPOs were incorporated into a single conical PET nanochannel substrate (CPOS-PET) *via* an in situ growth method (Fig. 3c), the obtained nanometer-to-subnanometer channels presented remarkable transport selectivity toward K<sup>+</sup>. The selectivity was calculated to be up to 31.6 and 363.8 for K<sup>+</sup>/Na<sup>+</sup> and K<sup>+</sup>/Li<sup>+</sup>, respectively (Fig. 3d). Meanwhile, the transport rate of K<sup>+</sup> through these crystal nanochannels reached  $9.44 \times 10^{-2} \text{ mol m}^{-2} \text{ h}^{-1}$ , which is two orders of magnitude higher than that of Na<sup>+</sup> and Li<sup>+</sup>. Simulations and experimental investigations further revealed that the underlying cation- $\pi$  and electrostatic interactions between K<sup>+</sup> ions and binding sites in the CPOS pores result in ultraselective K<sup>+</sup> transport and ion sieving.

As another important biological ion channel, the sodium (Na<sup>+</sup>) channel, as the name suggests, is highly

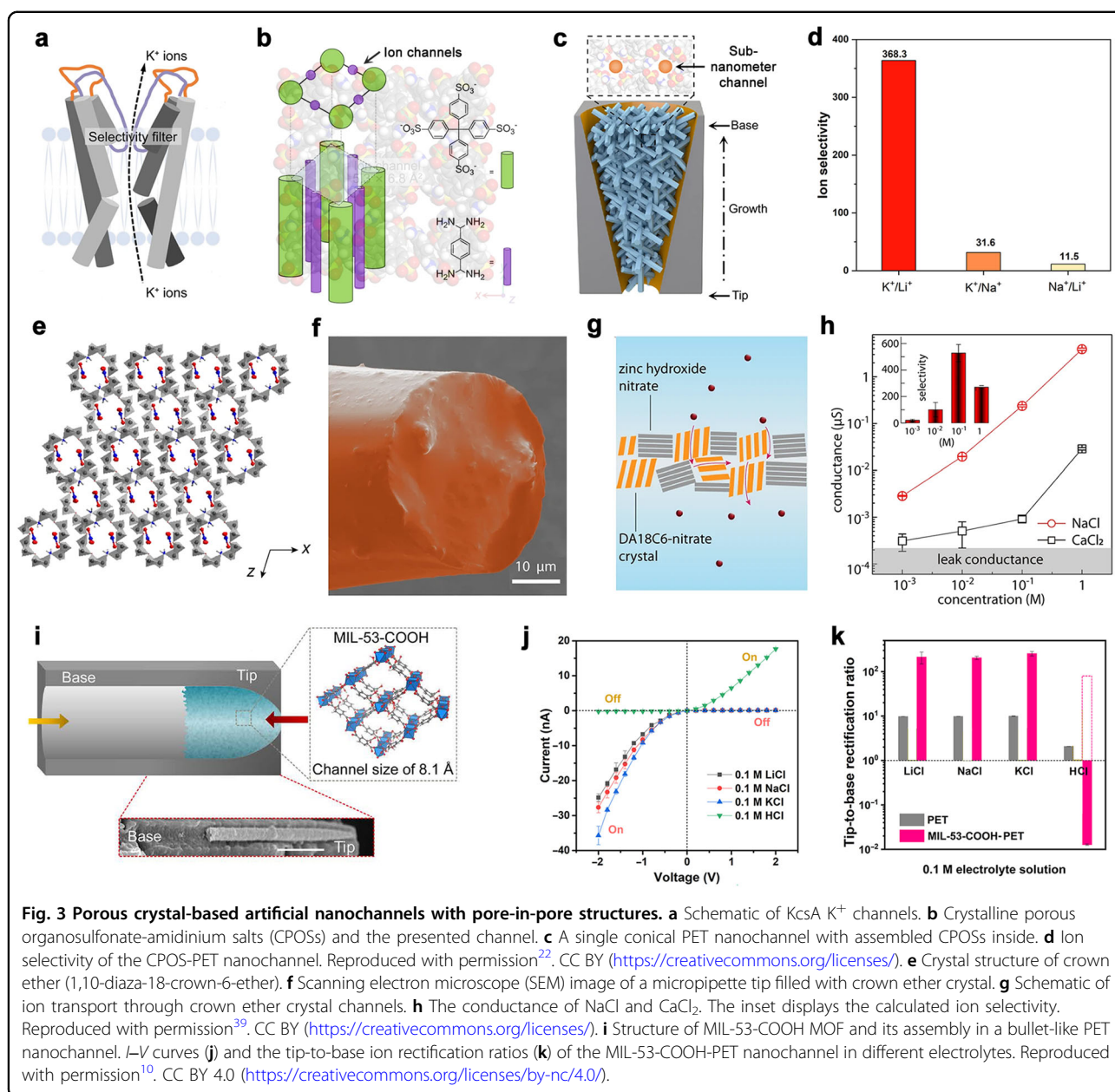


selective for the transport of  $\text{Na}^+$  ions across cell membranes, with a  $\text{Na}^+/\text{K}^+$  selectivity of  $\sim 10\text{--}10^2$  and a  $\text{Na}^+/\text{Ca}^{2+}$  selectivity of  $\sim 7$ . To reproduce the  $\text{Na}^+$  channel, Ye et al. investigated a nanoporous crown-ether crystal (Fig. 3e), which presents a cavity of  $\sim 2.6 \text{ \AA}$  that is larger than the  $\text{Na}^+$  diameter but smaller than  $\text{K}^+$ , as well as a strong  $\text{Na}^+$  affinity<sup>39</sup>. After the crown-ether crystal filled the tip of a quartz micropipette (Fig. 3f), the ion selectivity was evaluated. The results suggest high  $\text{Na}^+$  selective transport behavior (Fig. 3g) relative to  $\text{Ca}^{2+}$  and  $\text{K}^+$ , demonstrating selectivities of 15 and 523 (Fig. 3h), respectively, which reach or even exceed the values of biological  $\text{Na}^+$  channels. The size effect and affinity recognition between  $\text{Na}^+$  and the crown-ether crystal contributed greatly to the underlying excellent selectivity. Combined, this type of superior ion transport property relying on nanoporous bulk crystals is free from the material dimensions, thus providing a methodology to construct artificial transport or sieving devices with varied length scales and spatial dimensions.

In addition, emerging nanoporous materials such as MOFs and COFs are also attractive candidates for ion transport and sieving, owing to their intrinsic high porosity, ordered channels, and rich functional groups. Among these, 3D interconnected channels make the MOF and COF crystals a type of potential ion channel carrier similar to porous organic salt crystals. In 2020, Li et al.

assembled MOF crystals into a single PET nanochannel and built a heterostructured nanochannel system with a pore-in-pore structure, which achieved unidirectional and selective proton transport<sup>40</sup>. This work opens a new way to construct 1D nanochannels based on porous crystals with superior ion transfer properties. Subsequently, these researchers probed subnanochannels from the positively charged zirconium-based UiO-66-X ( $X = \text{H}, \text{NH}_2$ , or  $\text{N}^+(\text{CH}_3)_3$ ) MOF grown in situ in a PET nanochannel<sup>19</sup>. The results show an ultrahigh  $\text{F}^-$  conductivity of  $\sim 10 \text{ S m}^{-1}$  and ultrahigh  $\text{F}^-/\text{Cl}^-$  selectivity ranging from  $\sim 13$  and  $\sim 240$ , which primarily benefits from the electropositivity of the MOF and the specific interaction of  $\text{F}^-$  with the subnanometer-sized MOF channel.

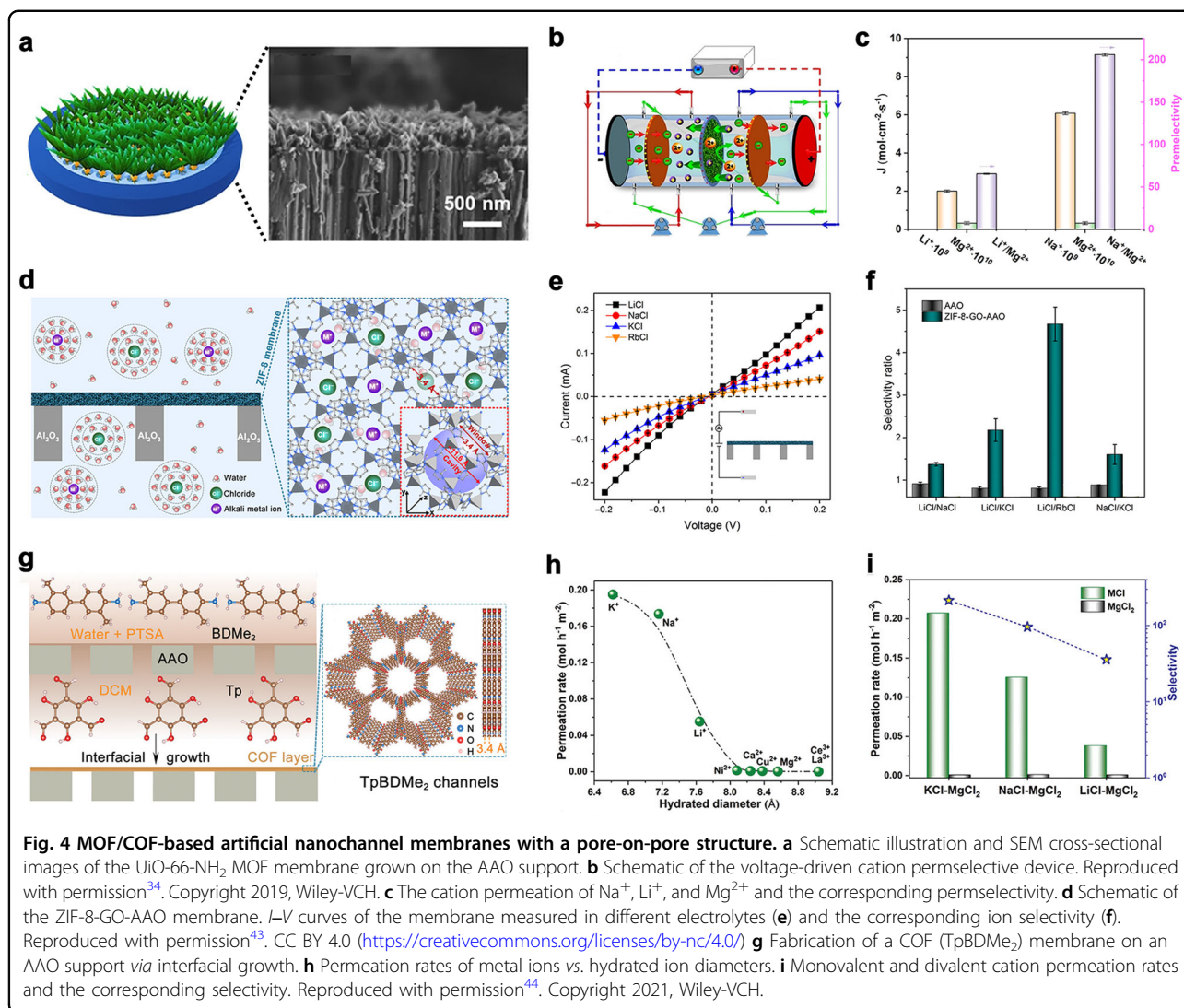
If the MOF is negatively charged, then can the corresponding channel achieve the selective transport of cations? To answer this question, Lu and coworkers built an asymmetrically structured MOF-based subnanochannel system by assembling a negatively charged UiO-66-(COOH)<sub>2</sub> MOF into a single bullet-like PET channel (denoted as UiO-66-(COOH)<sub>2</sub>-PET)<sup>23</sup>. Due to the asymmetric structure and surface charge distribution of the channel inside, this type of subnanochannel presented remarkable ion rectification effects toward three monovalent cations:  $\text{K}^+$ ,  $\text{Na}^+$ , and  $\text{Li}^+$ . Experimental and modeling evidence indicated that the selective transport of the monovalent cation of this UiO-66-(COOH)<sub>2</sub>-PET



shares several features, such as dehydration, affinity interaction, and structural flexibility, that are analogous to biological K<sup>+</sup> channels. Most recently, their group developed another type of asymmetric MOF-based nanochannel system that is composed of MIL-53-COOH MOF with the same strategy (Fig. 3i)<sup>10</sup>. This nanofluidic system also exhibited the excellent tip-to-base rectifying effect for Na<sup>+</sup>, K<sup>+</sup>, and Li<sup>+</sup> (Fig. 3j). The corresponding rectification ratios are far better than those of the previous MOF subnanochannels. It is surprising that the proton displays a reversed rectifying effect from base to tip, and the rectification ratio is up to 78.5 from the potential of +2 to -2 V (Fig. 3k). In addition, this

nanofluidic system also achieved an ultrafast proton permeability of 4.3 m s<sup>-1</sup>, which is considerably superior to other artificial proton channels. Theoretical simulations have suggested that a low energy barrier and ultrahigh proton permeability in the base-to-tip direction contributed to the substantial proton transport ability of the MOF-based subnanochannels. Thus, this unidirectional ultrafast counterdirectional transport of alkali metal cations and protons shows superior artificial control power.

Artificial ion channels with ultrafast ion transport and selectivity are urgently needed in ion sieving and separation, energy transformation, and sea water desalination



applications. Although subnanometer-sized channels that are assembled in a single microchannel have achieved ultrafast and superselective ion transport, their ion flux remains subject to a single microchannel and thus cannot meet the demand of practical applications that acquire high ion flux<sup>41</sup>. The key to a successful application is to prepare a defect-free and stable membrane containing abundant subnanometer-sized channels on a large scale. To fabricate defect-free and robust membranes, the in situ growth of porous crystals on microchannel membranes is a reasonable strategy. In this respect, Guo et al., by adopting a self-confined growth method, constructed a heterogeneous membrane with a pore-on-pore structure that consists of single-strand DNA threaded ZIF-8 MOF subnanochannels and the AAO supporting membrane<sup>42</sup>. The introduction of DNA significantly facilitated proton conductivity by the hydrogen bonding network structure. The subnanometer-sized cavities of ZIF-8 effectively

blocked methanol permeability, which renders the heterogeneous membrane an ideal candidate for proton exchange membranes in direct methanol fuel cells. Despite the use in the special scenario, the doping of a polymer in the porous crystal layer inevitably affects the ion flux. Thus, Xu and coworkers prepared a UiO-66-NH<sub>2</sub> leaf-like membrane on an AAO support (Fig. 4a) via an in situ growth method<sup>34</sup>. The density and thickness of the MOF layer can be readily tuned by altering the reaction conditions. The AAO pore aperture can also change to boost the ion permeability. The ion permeability of the obtained membranes was examined by using a potential-driven cation permeation cell (Fig. 4b). When the AAO pore size was approximately 90 nm and the MOF layer had a high density and a thickness of less than 500 nm, the heterogeneous membrane exhibited excellent permselectivity for Na<sup>+</sup> and Li<sup>+</sup> relative to divalent Mg<sup>2+</sup>, giving corresponding selectivity values of >200 for Na<sup>+</sup>/

$\text{Mg}^{2+}$  and  $>60$  for  $\text{Li}^+/\text{Mg}^{2+}$  (Fig. 4c). Moreover, this type of heterogeneous membrane also suggests superior long-term stability under harsh conditions with sea water, which thus demonstrates the great potential in the extraction of valuable metal cations.

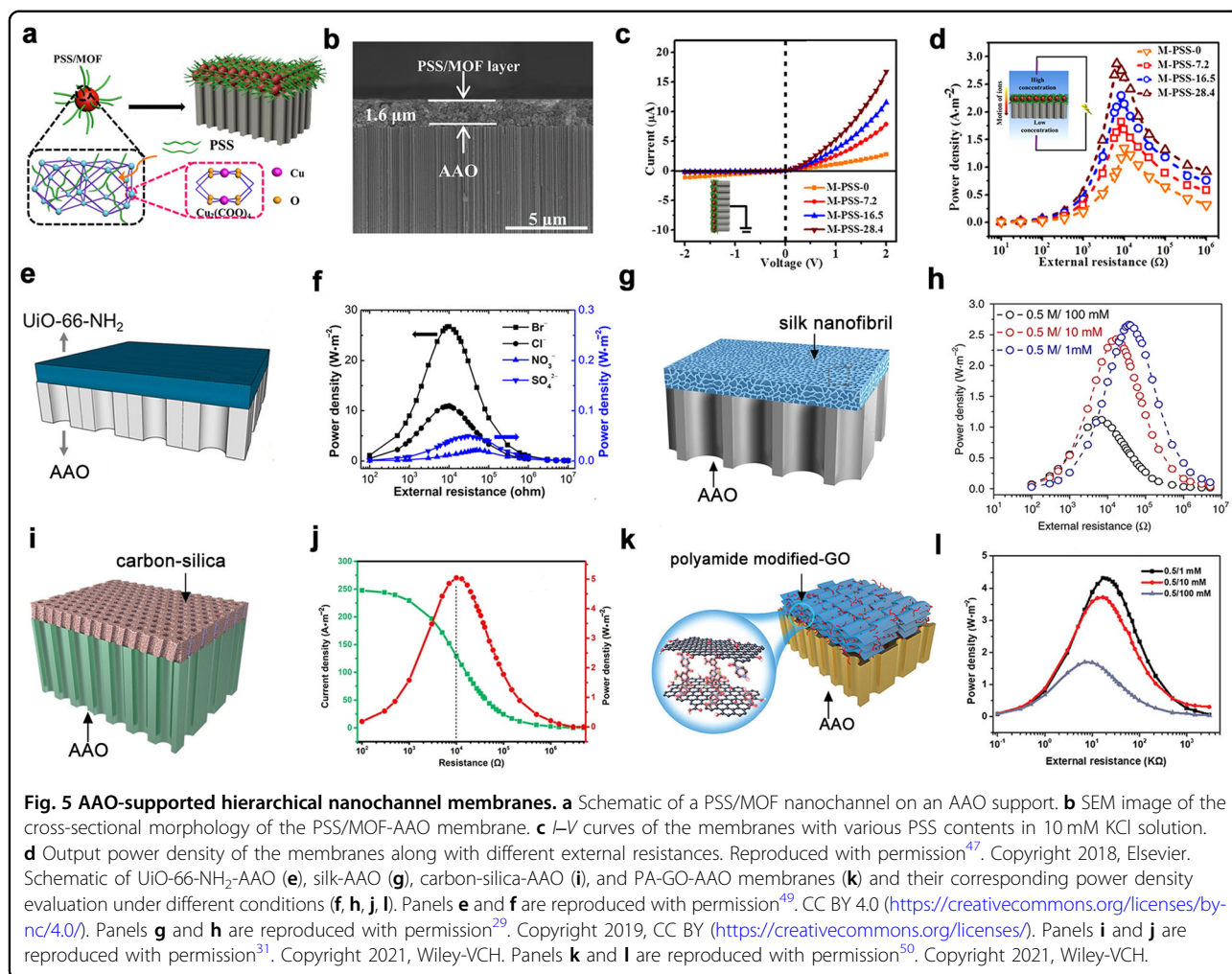
To achieve the efficient separation of monatomic alkali metal ions with the same valence and similar sizes, Zhang et al. developed a ZIF-8 subnanochannel membrane (Fig. 4d) via a nanoporous graphene oxide-assisted interfacial growth method on an AAO support (denoted as ZIF-8-GO-AAO)<sup>43</sup>. The thickness of the ZIF-8-GO membrane was approximately 446 nm. The conductance ratio obtained from the  $I$ - $V$  curves was used to characterize the ion selectivity of the ZIF-8-GO-AAO membrane (Fig. 4e). The results show the remarkable difference in ion transport of the ZIF-8-GO-AAO membrane. The order of the ion transport rate agrees well with the atomic number order (i.e.,  $\text{Li}^+ > \text{Na}^+ > \text{K}^+ > \text{Rb}^+$ ). Among these, the  $\text{Li}^+/\text{Rb}^+$  selectivity displays the highest value of 4.6 (Fig. 4f), benefiting from the fast and selective transport of  $\text{Li}^+$  over other alkali metal ions through the membrane based on unhydrated size exclusion.

Note that the pores of ZIF-8 are neutral and lack functional groups and thus generally cannot provide the specific ion binding capacity to achieve higher selectivity. To address this issue, Sheng et al. recently reported an AAO-supported COF (TpBDMe<sub>2</sub>) membrane<sup>44</sup>. By using an interfacial growth strategy, an ultrathin ( $\approx 20$  nm) COF membrane that possesses a pore size of 1.4 nm and abundant hydrogen bonding sites along the channel walls was constructed on an AAO support (Fig. 4g). The COF-AAO membrane has high monovalent cation permeation rates of  $0.1$ – $0.2$  mol m<sup>-2</sup> h<sup>-1</sup> as well as low multivalent cation permeabilities, as shown in Fig. 4h, resulting in remarkable mono/divalent cation selectivity for  $\text{K}^+/\text{Mg}^{2+}$  of  $\sim 765$ ,  $\text{Na}^+/\text{Mg}^{2+}$  of  $\sim 680$ , and  $\text{Li}^+/\text{Mg}^{2+}$  of  $\sim 217$  (Fig. 4i). The higher ion permeation is attributed to the sub-2 nanochannel of the COF. The high ion selectivity benefits more from the stronger hydrogen bonding interaction of the COF nanochannels with hydrated divalent cations than with monovalent cations. In general, these studies are beneficial for the development of diverse multifunctional ion channel membranes for ion sieving applications. It is worth noting that the porous crystal-based hierarchical nanochannel systems on the AAO support mentioned above did not exhibit a strong ion rectifying effect, probably because of the existence of some unavoidable defects. A porous carbon membrane possessing a hierarchical pore architecture reported by Lu et al. showed an ultrahigh ionic rectification ratio of up to  $1 \times 10^4$ , which, in other words, achieved quasi-unidirectional ion transport with an artificial nanochannel<sup>45</sup>. Thus, the chemical vapor deposition (CVD) method they adopted might be more appropriate to construct ion unidirectionally transported membranes.

## Osmotic energy harvesting

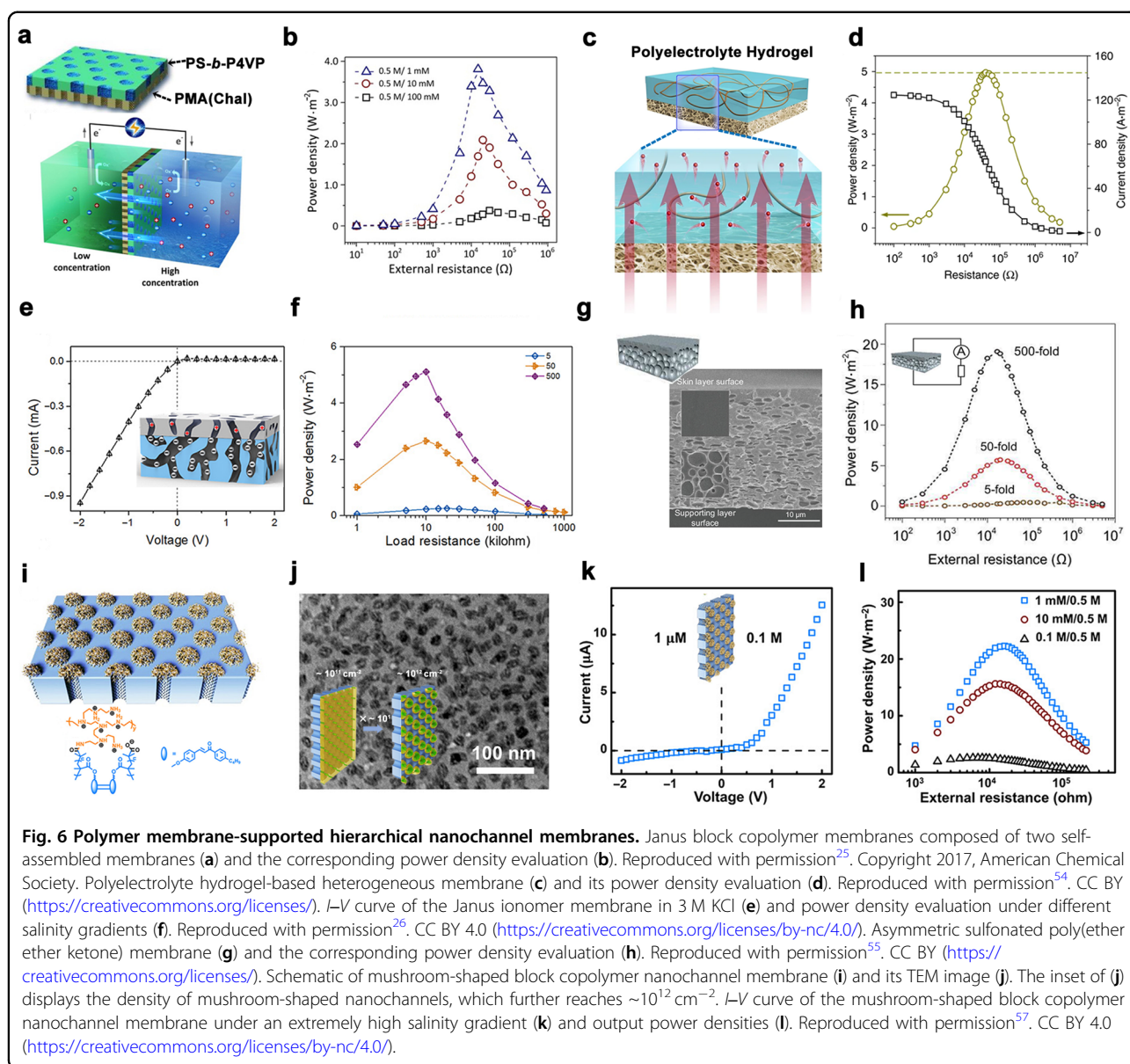
The osmotic energy that exists widely at the junction of seawater and river water is a potential large-scale renewable and sustainable energy source. However, current osmotic energy conversion processes only supply limited power output due to the poor power density stemming from the intrinsic high resistance of conventional ion-exchange membranes. It has been predicted that a hierarchical nanochannel membrane with a strong ionic current rectification property could be a very efficient material<sup>26</sup>. Therefore, many hierarchical nanochannel membranes have been constructed for the purpose of osmotic energy harvesting over the past few years.

AAO and track-etched porous PET membranes featuring highly arranged nanochannels are usually used as the supporting layers of hierarchical nanochannel membranes due to their variable and controllable channel structures and favorable stability<sup>30,46</sup>. In 2018, Li et al. demonstrated a series of hybrid nanochannel membranes constructed by combining polystyrene sulfonate (PSS)/MOF composites with an AAO support (Fig. 5a)<sup>47</sup>. The PSS/MOF-AAO composite membrane (Fig. 5b) shows abundant channels from the MOF and a high density of functional groups from polymers. The ion transport behaviors of the nanochannel membranes with varying PSS content were examined by  $I$ - $V$  curves in 10 mM KCl electrolyte solution. As displayed in Fig. 5c, the optimized membranes with 28.4% PSS exhibited the most obvious ion current rectification with a ratio value of approximately 98. This strong rectification mainly resulted from the geometrical (microchannel of AAO layer vs. nanochannels of PSS/MOF layer) and electrostatic (positive charges of AAO microchannel surface vs. rich negative charges of the nanochannel surface of PSS/MOF layer) asymmetries. After integrating it into an osmotic energy conversion device, a power output of  $2.87$  W m<sup>-2</sup> can be achieved in an artificial seawater (0.5 M NaCl)/river water (0.01 M NaCl) system (Fig. 5d), which shows great promise for practical applications. Since MOF-based hybrid membranes can provide effective control over ionic transport, several MOF-based membranes have also been developed as osmotic power generators<sup>33,48</sup>. However, the output performance of these membranes is not always ideal. In 2021, Liu et al. fabricated a UiO-66-NH<sub>2</sub>-AAO heterogeneous membrane (Fig. 5e)<sup>49</sup>, which produced an exceptionally high  $\text{Br}^-/\text{NO}_3^-$  selectivity of  $\sim 1240$  and achieved an unprecedented power density of up to  $26.8$  W m<sup>-2</sup> under a 100-fold KBr gradient (Fig. 5f). The high positively charged and rich angstrom-scale (ca. 6 to 7 Å) windows and nanometer-scale cavities in the UiO-66-NH<sub>2</sub> layer contributed to the unexpected but outstanding osmotic transport properties. However, the maximum output power density achieved was only



$7.12 \text{ W m}^{-2}$  under a 500-fold KCl gradient, mainly because  $\text{Br}^-$  ions with a smaller hydrated diameter can be more easily transported into the nanochannel in the UiO-66-NH<sub>2</sub> layer with positive charges. Given that these hierarchical nanochannel membranes still suffer from high cost and complex preparation, scientists have been pursuing membrane materials with stability and high efficiency from common natural biomaterials. By using cellulose nanofibers, Xu et al. prepared a nanoporous nanofiber-based layer on a conical porous PET support<sup>28</sup>. The optimized heterogeneous membranes exhibit an ultrahigh ion current rectification ratio of 562. However, the output power density is relatively low, only  $0.96 \text{ W m}^{-2}$  in 0.5 and 0.01 M NaCl solutions. In addition, Xin et al. utilized natural silk fiber to form a thermodynamically stable structure and constructed a silk-AAO heterochannel membrane (Fig. 5g). This membrane achieved long-term stability as well as high power conversion ability with a power density of  $2.86 \text{ W m}^{-2}$  at a 50-fold NaCl gradient (Fig. 5h)<sup>29</sup>, which demonstrates the superiority of natural materials.

With the advancement of interfacial superassembly methods, many novel heterostructure membranes have been constructed by driving guest materials to a substrate through noncovalent bonds. Based on this, Zhou et al. constructed a mesoporous silica-AAO hybrid membrane, which revealed a power density of  $4.50 \text{ W m}^{-2}$  under the conditions of artificial seawater and river water<sup>30</sup>. Furthermore, their team improved its ionic selectivity and stability performance by introducing a two-component mesoporous “reinforced concrete”-structured carbon-silica layer on an AAO support (Fig. 5i)<sup>31</sup>. The ordered two-component nanochannel layer with high surface charge endowed the membrane with enhanced cationic permselectivity as well as a temperature- and pH-sensitive salinity gradient energy conversion capacity. A high output power density of  $5.04 \text{ W m}^{-2}$  (Fig. 5j) was obtained. Due to the emergence of a facile and efficient superassembly strategy, graphite oxide (GO)-based heterochannel membranes, which were difficult to prepare before, are now available. In 2021, Zhang et al. constructed a GO-based heterochannel membrane, that is, a



polyamide-modified GO membrane, on an AAO support (denoted PA-GO-AAO) (Fig. 5k), which exhibited a good osmotic energy conversion ability with a power density of up to  $3.73 \text{ W m}^{-2}$  (Fig. 5l)<sup>50</sup>. Similar to other hierarchical nanochannel systems in the mechanism, the asymmetric charge distribution and geometrical nanochannel structure are responsible for the good directional ionic rectification features and the outstanding cation selectivity.

Hierarchical nanochannel membranes consisting of heterogeneous porous polymers with different nanopore sizes have also been exquisitely designed for osmotic energy conversion<sup>26,27,51,52</sup>. Amphiphilic block copolymers bearing multifunctional macromolecular blocks can form porous polymers with well-defined mesopore structures, thus providing an ideal candidate for the

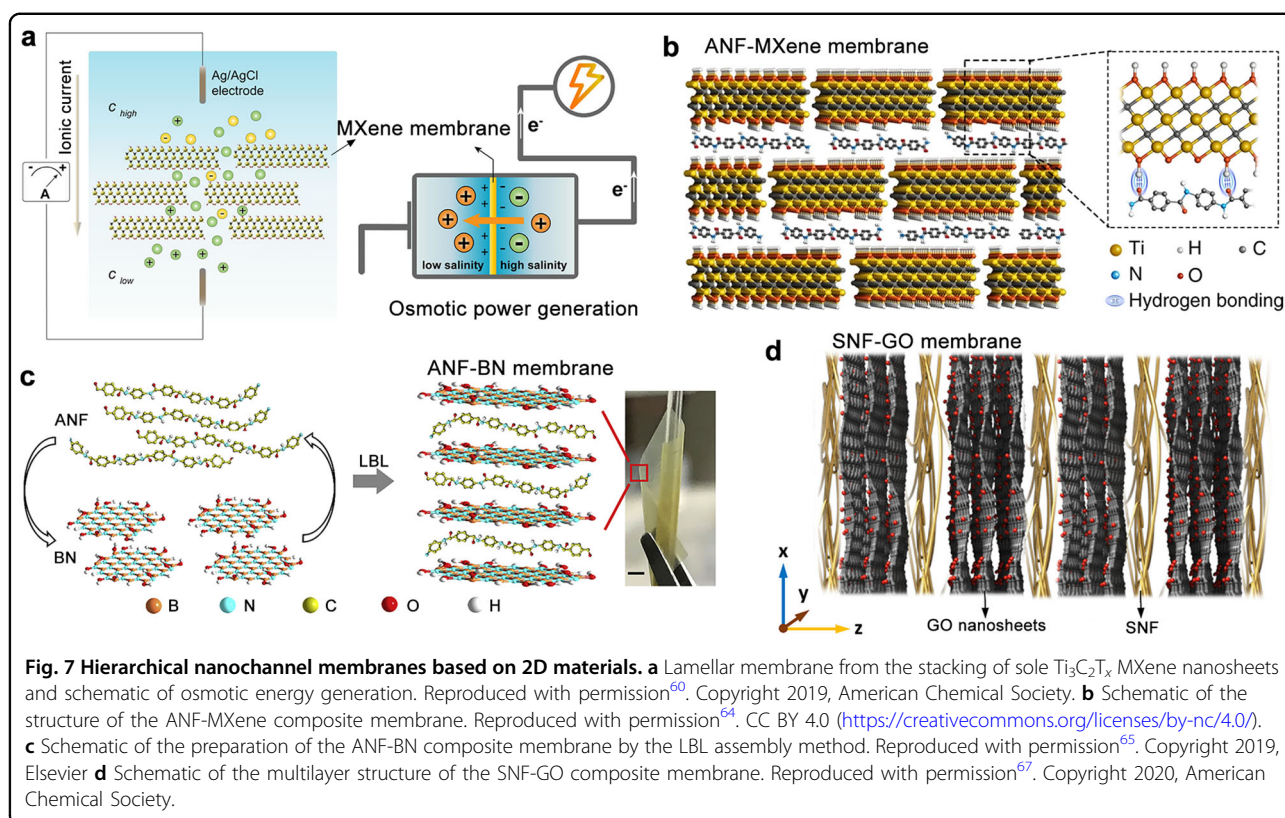
construction of nanochannel membranes<sup>25,53</sup>. In this respect, Zhang et al. presented a Janus block copolymer heterogeneous nanochannel membrane composed of two self-assembled layers that both exhibit hexagonally packed pores (Fig. 6a)<sup>25</sup>. The opposite charge distribution and asymmetric channel architecture contributed to selective ionic transport, which finally achieved osmotic energy conversion with a power density of approximately  $2.04 \text{ W m}^{-2}$  (Fig. 6b) by mixing natural seawater and river water. However, the unsatisfactory power density may enable a low interfacial ion transport efficiency caused by the mismatch of pore alignment and inappropriate coupling between channels of different dimensions at the interface. Thus, to improve the power output, these researchers prepared a heterogeneous membrane with a

polyelectrolyte hydrogel interface by coating functional polyelectrolyte hydrogel onto the supporting porous aramid nanofiber membrane (Fig. 6c)<sup>54</sup>. The polyelectrolyte hydrogel layer possessing many negatively charged sulfonate groups can act as an ion accelerator to greatly increase the ion transport efficiency. Such a heterogeneous membrane outputs a power density of  $5.06 \text{ W m}^{-2}$  by mixing seawater and river water (Fig. 6d). Moreover, considering the energy loss caused by the polarization phenomenon during the conversion process, Zhu et al. tried to use a porous Janus ionomer membrane with nonlinear transport to inhibit backward current and achieved low energy dissipation and high performance in osmotic energy harvesting (Fig. 6e)<sup>26</sup>. The porous Janus-type ionomer membrane can maintain high rectification even in a hypersaline environment, giving a power density of  $5.10 \text{ W m}^{-2}$  in a 500-fold salinity gradient (Fig. 6f).

Osmotic energy harvesting membranes with high performance as well as facile synthesis methods are always the pursuit of scientists. In 2020, Zhao and coworkers prepared a sulfonated poly(ether ether ketone) membrane through a simple nonsolvent-induced phase separation method<sup>55</sup>. The obtained polymer membrane consists of a thin skin layer with a smooth surface as well as a negatively charged nanochannel and a sponge-like supporting layer with abundant interconnected hierarchical pores, showing an obvious asymmetric structure (Fig. 6g). When the polymer membrane was applied to osmotic energy harvesting, an output power density of  $5.8 \text{ W m}^{-2}$  (Fig. 6h) was achieved under a salinity gradient of 0.5 M/0.01 M. The power density was further increased to  $7 \text{ W m}^{-2}$  by doping MOF nanosheets into the polymer matrix because the incorporation of MOF nanosheets increases the ion flow rate in a confinement region<sup>56</sup>. These records were broken until 2021 by a mushroom-shaped nanochannel membrane with an ultrathin selective layer on a block copolymer self-assembled nanochannel array<sup>57</sup>. As shown in Fig. 6i, the stem part of the mushroom-shaped structure is a negatively charged nanochannel array with a density of  $\sim 10^{11} \text{ cm}^{-2}$ . The cap part is a positively charged channel network formed by single-molecule-layer hyperbranched polyethyleneimine. This overlaying structure significantly elevated the nanochannel density to  $\sim 10^{12} \text{ cm}^{-2}$  (Fig. 6j), endowing the membrane with excellent ion selectivity and unidirectional ion transport properties (Fig. 6k). The evaluation results show that the membrane can generate an output power density of up to  $22.4 \text{ W m}^{-2}$  under a 500-fold salinity gradient (Fig. 6l). Combined, these hierarchical nanochannel membranes open promising prospects for large-scale osmotic energy conversion. These diverse heterogeneous nanochannel membranes also provide abundant resources and inspiration for the exploitation and utilization of osmotic energy.

Recently, nanofluidic membranes constructed from 2D materials have increasingly aroused interest in the field of osmotic energy conversion. In theory, an atomically or molecularly thin 2D membrane with nanopores can remarkably decrease the internal resistance of the membrane and enhance the ion conductivity, thus displaying potential as an excellent ion-selective nanofluidic device. For example, a single-layer nanoporous carbon membrane with nanopores of  $3.6 \pm 1.8 \text{ nm}$  in pore diameter exhibits supreme ion conductivity and a remarkable output power density of  $67 \text{ W m}^{-2}$  in a reverse electro dialysis test<sup>58</sup>. Similarly, a metal tetraphenylporphyrin-based COF (MTPP-COF) monolayer membrane with an innate nanopore array as the osmotic power generator achieved an output power density over  $200 \text{ W m}^{-2}$  in an artificial seawater and river water system<sup>59</sup>. Despite the outstanding output power density, this type of single-layer nanoporous membrane is always subject to difficulties in scalable preparation. Lamellar membranes fabricated by stacking 2D nanosheets are an alternative solution, which makes full use of the interplanar nanochannels to transport ions and offers the possibility to scale up for membrane production. For instance, the lamellar  $\text{Ti}_3\text{C}_2\text{T}_x$  MXene membrane is reported to achieve an output power density of  $21 \text{ W m}^{-2}$  at a 1000-fold salinity gradient (Fig. 7a)<sup>60</sup>. In addition, other lamellar membranes based on GO<sup>61</sup>, carbon nitride ( $\text{C}_3\text{N}_4$ )<sup>62</sup>, and boron nitride (BN)<sup>63</sup> also exhibit dramatic ion transport performance.

However, many lamellar 2D nanosheet membranes easily disintegrate in aqueous solution and lose their stratified structure and thus cannot meet the requirement for long-term stability. To enhance the robustness of 2D-material-based membranes, researchers have explored integrating 1D fibers as intercalating and interlocking agents into 2D nanosheet membranes. In this regard, Zhang and coworkers fabricated a composite membrane with a hierarchical nanochannel architecture based on 2D  $\text{Ti}_3\text{C}_2\text{T}_x$  MXene nanosheets and 1D aramid nanofibers (ANFs) by a vacuum-assisted filtration method (Fig. 7b)<sup>64</sup>. Benefiting from the synergetic effect of the surface negative charge of MXene and the space negative charge of ANF, this composite membrane shows strong cation-selective transport. In a natural sea/river water system, the output power density of this membrane can achieve  $4.1 \text{ W m}^{-2}$ . This work highlights the important role of space charge in the nanoconfinement of the interstitial space between 2D nanosheets. Based on a similar concept, Chen et al. adopted a layer-by-layer (LBL) assembly method and constructed hierarchical composite membranes based on 1D AFN and 2D BN (denoted as AFN-BN membrane) (Fig. 7c)<sup>65</sup> or GO nanosheets (denoted as AFN-GO membrane)<sup>66</sup>. These two membranes show good mechanical strength and long-term robustness, and their osmotic energy harvesting ability is comparable to



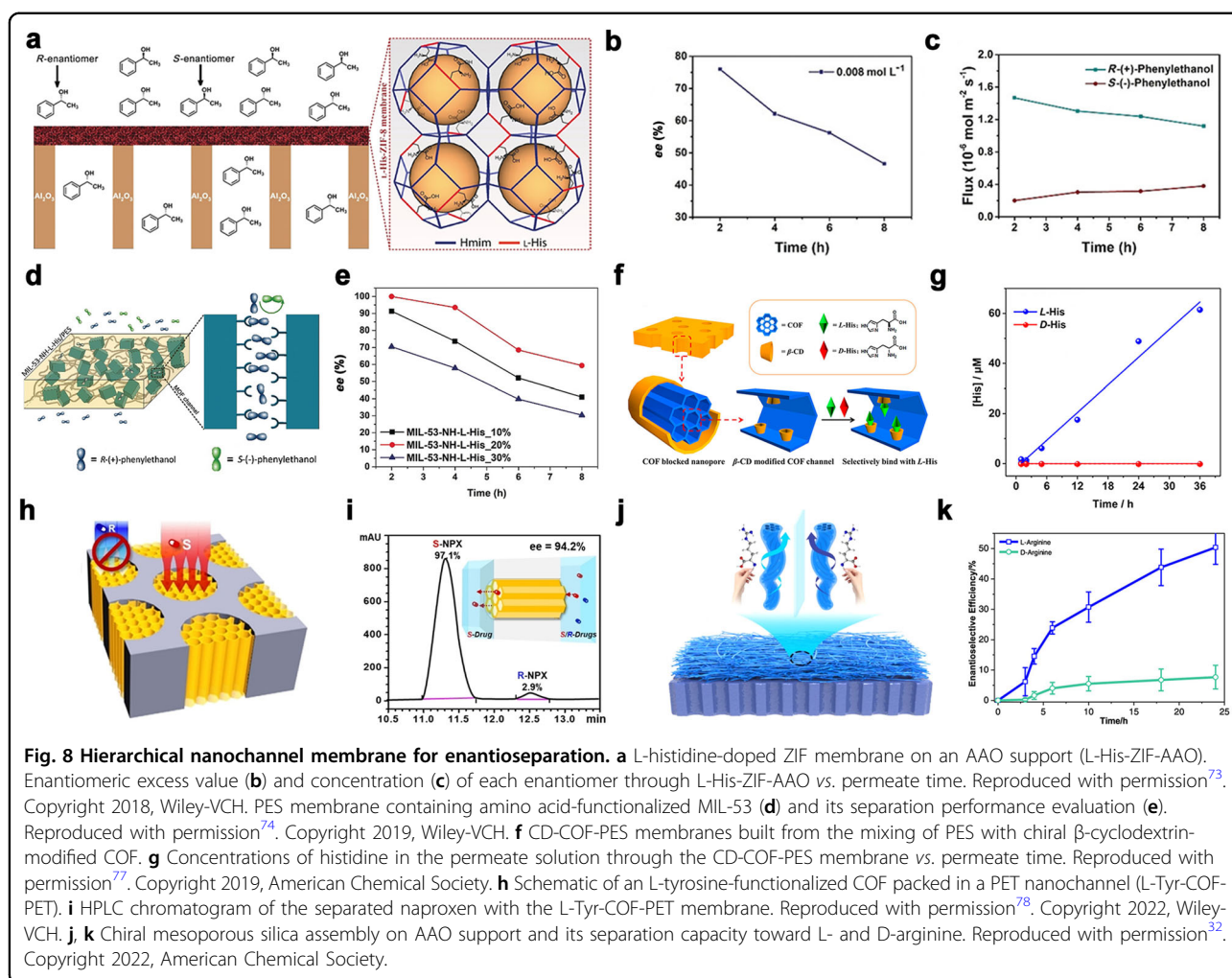
that of reverse electrodialysis (RED) devices. The ultra-strong AFN-GO membrane can even harvest salinity gradient energy from organic solutions. In addition, Xin et al. incorporated natural silk nanofibers (SNFs) into GO nanosheets to build an SNF-GO hierarchical nanofluidic membrane (Fig. 7d)<sup>67</sup>. The nacre-like multilayer sandwich architecture from the interlocking between SNFs and GO endows this hierarchical membrane with strong mechanical strength and stability. Osmotic energy tests showed that this membrane achieved a power density of  $5.07 \text{ W m}^{-2}$  in a sea/river water system, which reached the criterion of at least  $5.0 \text{ W m}^{-2}$  for industrial applications. In summary, these studies provide inspiration for the development of available materials that comprehensively consider the membrane strength, robustness, power density, ease of scale up, cost, etc.

### Enantioseparation and biosensing

Nanochannels with precisely controlled structures and customizable interfacial chemistry analogous to biological ion channels are potential candidates for bioseparation and biosensing with high selectivity. The separation and sensing selectivity of nanochannel membrane materials at the molecular level is mainly based on the molecular properties (size, charge, and lipophilicity) as well as interactions between molecules and nanochannels<sup>68,69</sup>. Therefore, the selectivity can be tuned by size control and

proper modification of the nanochannels<sup>70</sup>. Accordingly, designing and controlling the nanochannel architecture in terms of the 3D geometrical parameters and 2D surface chemical features present opportunities for the development of novel heterochiral nanochannel platforms for bioseparation and biosensing<sup>71,72</sup>.

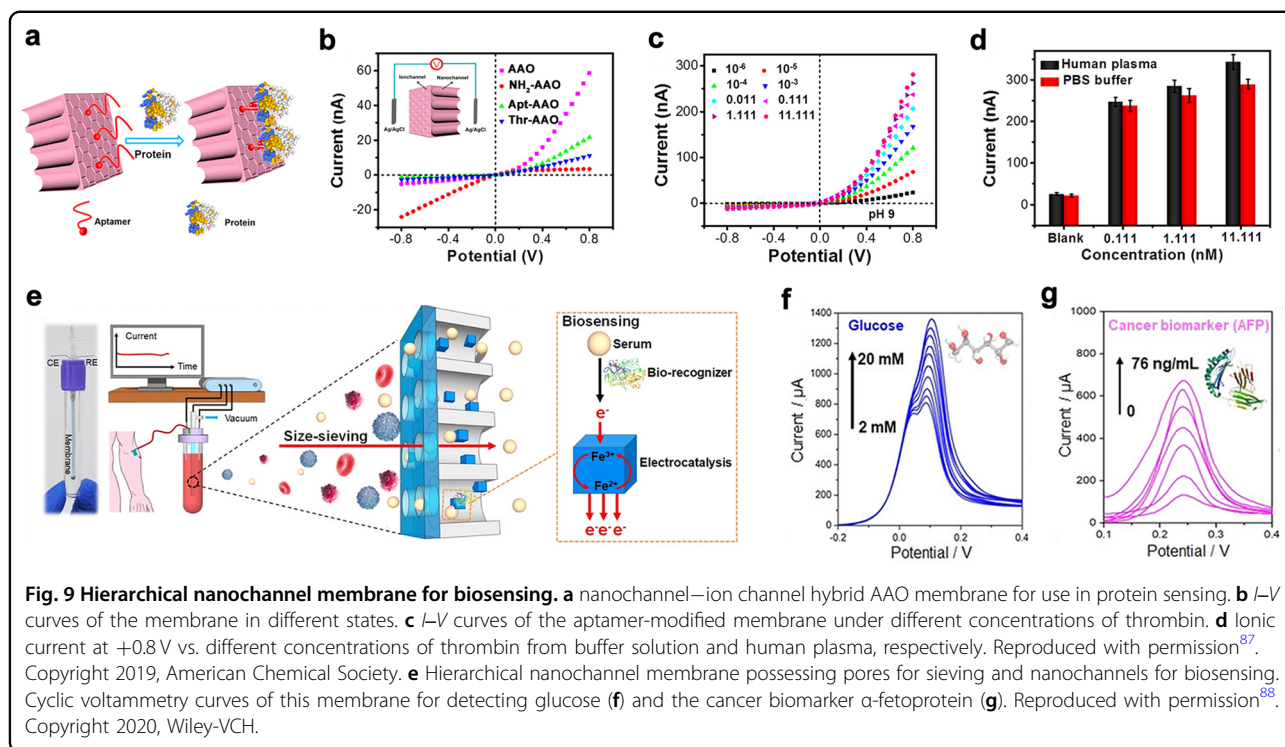
Emerging homochiral MOFs and COFs with controllable pores have proven to be desirable platforms for chiral separation<sup>69</sup>. In 2018, Chan et al. constructed a homochiral MOF layer on a porous AAO support by integrating L-histidine into the ZIF-8 framework (denoted as L-His-ZIF-AAO) with a contradiffusion method (Fig. 8a)<sup>73</sup>. Among these compounds, L-histidine functions as a chiral selector. Chiral resolution test results indicated that the highest enantiomeric excess (*ee*) value of 76% was obtained with the *R*-enantiomer in excess (Fig. 8b). As diffusion proceeded, the concentration of *R*- (+)-1-phenylethanol remained higher than that of *S*- (-)-1-phenylethanol (Fig. 8c). This result suggests that the L-His-ZIF-AAO membrane has good selectivity for the *R*-enantiomer of 1-phenylethanol. Subsequently, their group tried to construct chiral membranes by embedding homochiral MOFs in a polymer network (Fig. 8d)<sup>74</sup>. Accordingly, the resulting polyethersulfone (PES) membranes containing amino acid functionalized MIL-53 as a chiral selector achieved an ultrahigh *ee* value of up to 100% for racemic 1-phenylethanol (Fig. 8e).



Chiral COF membranes also demonstrate potential for enantiomer separation<sup>75</sup>. However, for COF materials, it remains difficult to construct defect-free COF membranes to realize their full potential in separation due to their poor film-forming ability<sup>76</sup>. To tackle this problem, Yuan et al. incorporated  $\beta$ -cyclodextrin-modified COFs into a polyethersulfone matrix and fabricated a mixed matrix membrane (denoted CD-COF-PES) (Fig. 8f)<sup>77</sup>. Benefiting from the selective chiral recognition ability of CD elements to L-histidine, the nanochannel membrane can selectively transport L-histidine. Accordingly, the concentration of the transported L-histidine through the membrane increased continuously with time, which is in sharp contrast to the constant concentration of D-histidine (Fig. 8g). Recently, Zhang et al. tried to employ a nanochannel membrane that has the potential for large-scale separation to explore the enantioseparation capacity with high selectivity and high flux<sup>78</sup>. These authors packed L-tyrosine functionalized COF (denoted as L-Tyr-COF) into the nanochannels of PET (Fig. 8h) and obtained an L-Tyr-COF-PET heterogeneous

membrane with a pore-in-pore structure. L-Tyr-COF with a pore size of 2 nm endowed the membrane with, on the one hand, a size that matches the molecular size of naproxen enantiomers and, on the other hand, an excellent chiral recognition capacity from a large number of L-Tyr sites. The enantioseparation evaluation of racemic naproxen with the L-Tyr-COF-PET membrane revealed a high *ee* value of 94.2% (Fig. 8i). Most importantly, such a heterogeneous nanochannel membrane achieved an ultrahigh separation flux of  $1.13 \text{ mmol m}^{-2} \text{ h}^{-1}$ . This work balances the contradiction of chiral separation membranes between selectivity and flux, demonstrating their great potential in large-scale enantioseparation.

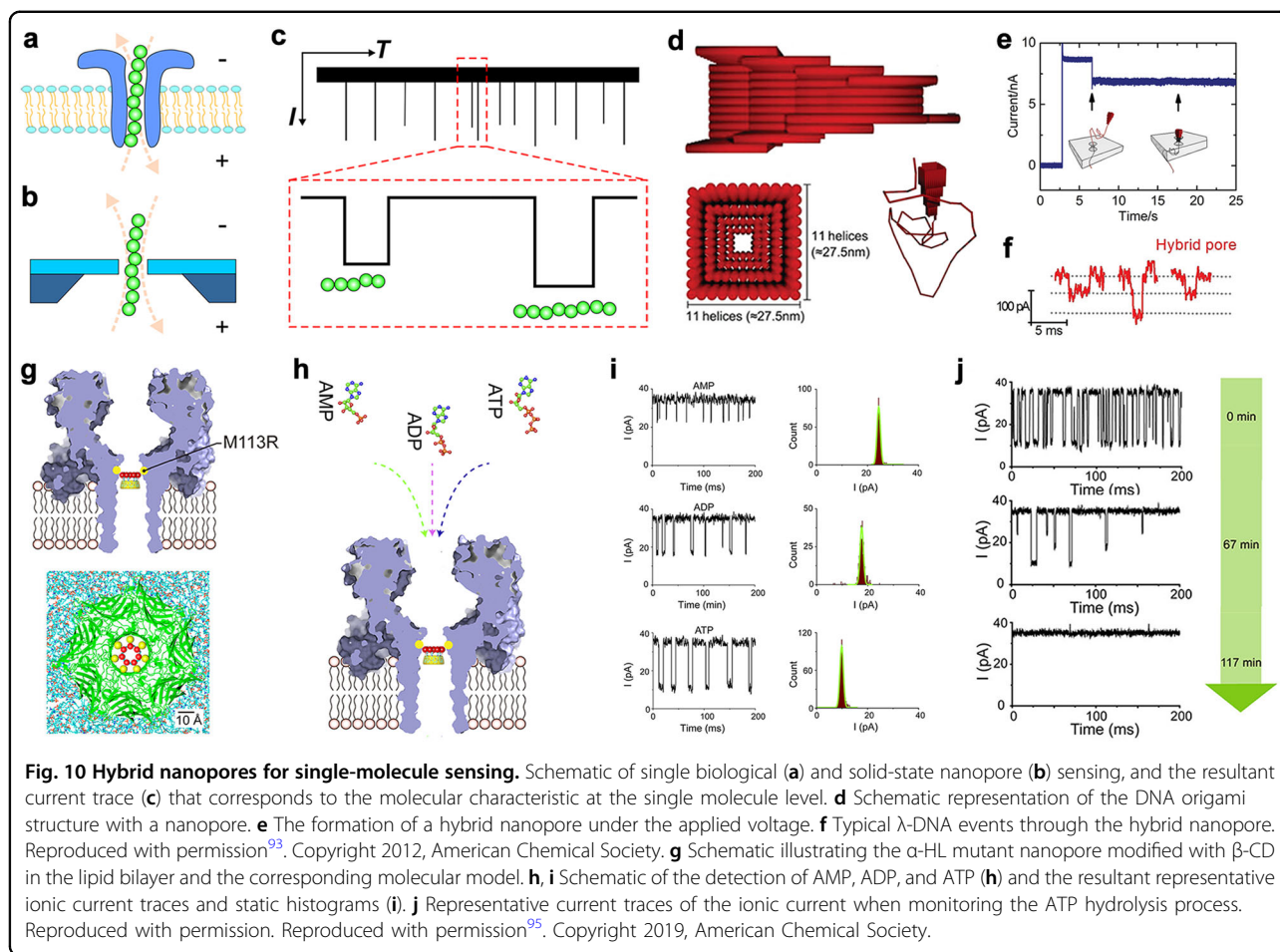
However, homochiral MOFs and COFs are still limited in terms of applications because of their complicated synthesis procedure. As an alternative, ordered mesoporous silica (OMS) has gained attention due to its simple synthesis, large surface area, and high stability. Recently, Cheng et al. fabricated a mixed-matrix membrane consisting of a polymer and chiral OMS by introducing L-alanine-pillar[5]arene to OMS<sup>79</sup>. This chiral OMS



membrane achieved the separation of *R*-propranolol. However, the introduction of chiral recognition elements through the postmodification of chiral ligands generally results in the problem of low modification efficiency. Thus, the abundant protogenous chiral elements in the synthesis of nanochannel membranes might be an optimum solution. In this regard, Huang et al. developed a heterostructured chiral membrane consisting of chiral helical-structured OMS supramolecular assemblies on an AAO support (denoted cOMS-AAO) (Fig. 8j)<sup>32</sup>. The obtained cOMS-AAO heterogeneous membrane shows superior cation selectivity, as well as an osmotic energy conversion of  $3.25 \text{ W m}^{-2}$ . The cation selectivity and chirality further endow the membrane with a stable enantioseparation capacity, especially for positively charged arginine molecules (Fig. 8k).

In addition, the excellent ion selectivity and asymmetric structure of hierarchical nanochannels also contribute to an ideal platform for biosensing. Prior to that, many artificial homogeneous nanochannels have been constructed sensors to detect carbohydrates<sup>80</sup>, peptides<sup>81,82</sup>, DNA<sup>83</sup>, proteins<sup>84</sup>, etc., by properly modifying functional elements to enhance biomolecule recognition selectivity<sup>85,86</sup>. The corresponding sensing mechanism mainly relies on the specific interaction of functional elements with the target analyte. However, these sensing systems based on homogeneous nanochannel supports do not work well in a complicated environment with the existence of many interfering substances. For hierarchical

nanochannels, in addition to the specific recognition interaction, the size sieving ability from the hierarchical channel architecture further endows the nanochannel with excellent selectivity for biomolecules of a specific size even in a complicated environment. In 2019, Zhao et al. prepared an aptamer-modified hierarchical AAO nanochannel membrane consisting of  $\sim 40$  nm nanochannels and subnanometer-sized ion channels (Fig. 9a)<sup>87</sup>, which combines the advantages of hierarchical nanochannels and specific modifications. This nanochannel membrane presents a fine rectification effect owing to its asymmetric structure (Fig. 9b) and can achieve the label-free detection of thrombin by taking advantage of the change in rectification. Under optimal conditions, the limit of detection can be as low as  $0.22 \text{ fM}$  (Fig. 9c). In addition, excellent biosensing performance in real samples was also achieved (Fig. 9d). In addition to chemical modification, another way to increase the biomolecule selectivity of artificial nanochannels is to reasonably tune their pore size. For example, Chu et al. constructed a hierarchical membrane consisting of a porous sieving layer with smaller nanopores and a biosensing layer with larger channels<sup>88</sup>. The sieving layer only allows serum to pass through by precisely controlling its pore size. Then, the biosensing layer with immobilized specific biorecognizers can realize the dynamic detection of objective biomolecules in serum without other interference, such as cells and fibrinogen in blood (Fig. 9e). By assembling the membrane in a portable device, online monitoring of glucose can be achieved



when glucose oxidase is immobilized in the biosensing channel (Fig. 9f). Furthermore, by introducing other kinds of biorecognizers in the large channels, cancer biomarkers can also be accurately sensed (Fig. 9g).

Over the past two decades, the field of single-molecule sensing with nanosized channels (referring to nanopores with a shorter axial length) has attracted widespread interest. Conceptually, a nanopore functions as a sole channel between both sides of electrolyte solutions (Fig. 10a, b). When an analyte molecule was driven across a nanopore, the steady ionic current was partially blocked, thus producing an analyte-specific single-molecule blockage signal (Fig. 10c). To date, a variety of biological nanopores and synthetic solid-state nanopores have shown great application potential in DNA sequencing, protein identification, biomolecular detection, etc.<sup>89,90</sup>. Notably, the suitable size of the nanopore that matches the molecular size of the analyte is the key to achieving remarkable nanopore sensing signals. Thus, great efforts have been made to prepare artificial nanopores with controllable pore shapes and pore properties. In this regard, the hierarchically engineered heterogeneous nanopore offers a solution to obtain applicative

nanopores<sup>91</sup>. For example, by inserting a biological protein nanopore into a solid-state nanopore, the hybrid nanopore system can facilitate the integration of wafer-scale nanopore arrays with controllable and unified pore sizes<sup>92</sup>. Beyond the fixed size of biological nanopores, Bell et al. turned their attention to a DNA origami structure because it can create an arbitrary 2D or 3D architecture at the nanoscale<sup>93</sup>. A DNA origami structure with a funnel shape was designed with a long double-stranded DNA tail to aid trapping in the correct orientation (Fig. 10d). Under an applied voltage, the DNA origami structure was driven and docked to a solid-state nanopore (Fig. 10e). Then, the formed DNA nanopore assembly successfully sensed translocation events of linearized  $\lambda$ -DNA (Fig. 10f). This work contributed to the feasibility of creating a nanopore system with adaptable diameters and shapes.

Another challenge of current nanopore sensing lies in the recognition and capture of small biomolecules due to their fast translocation through nanopores and the lack of affinity of nanopores for analytes. As early as 1999, Gu et al. found that  $\beta$ -cyclodextrin ( $\beta$ -CD) could enter and fit into the lumen of the  $\alpha$ -hemolysin ( $\alpha$ -HL) nanopore, resulting in the partial blockage of ionic current<sup>94</sup>. In this

case, the feature of  $\beta$ -CD that generally acts as the host to various guest molecules makes it a single molecule adapter by virtue of the confined cavity of  $\beta$ -CD, which can sense some organic small molecules (e.g., adamantanes) by a stochastic sensing approach. Recently, Su and coworkers modified  $\beta$ -CD by introducing positively charged quaternary ammonium groups and realized strong and steady binding of the modified  $\beta$ -CD with the  $\alpha$ -HL mutant (M113R, Fig. 10g)<sup>95</sup>, which can maintain a stable blockage current for a long time ( $\sim 18.75$  s). This hybrid nanopore system can differentiate three typical adenosine phosphates (AMP, ADP, and ATP) (Fig. 10h, i) and monitor the ATP hydrolysis process (Fig. 10j) by a single-molecule sensing approach. Based on a similar strategy, the hybrid nanopore system combining  $\beta$ -CD and  $\alpha$ -HL can discriminate polysulfides with single-sulfur atom differences at the single-molecule level<sup>96</sup>. Therefore, these hybrid nanopore systems with pore-in-pore structures offer an inspiration to engineers and can refine current biological nanopores to achieve specific sensing toward an analyte of interest.

### Concluding remarks and perspectives

The exquisite structures of biological ion channels provide inspiration for designing and constructing artificial ion channels to achieve analogous functions. Compared with homogeneous and symmetric nanochannels with simple structures and monotonic functional groups, hierarchically engineered nanochannel systems have demonstrated superior properties derived from their well-designed hierarchical structures as well as diverse and multifunctional chemical components from different levels of hierarchical pores. Starting from the design rationales of two main types of hierarchical nanochannels, that is, pore-in-pore and pore-on-pore structures, we have presented hierarchically engineered nanochannels with different compositions, structures, and asymmetries. Furthermore, we discuss the basic properties of hierarchical nanochannels, including ionic selectivity and ionic rectification, which are closely related to their chemical compositions and physical structures. These unique properties make the hierarchically engineered nanochannel systems perform well in ion-selective transport and initiate applications in many fields, such as osmotic energy conversion, bioseparation, and biosensing.

Despite being mechanically and chemically more stable than protein-based biological ion channels, current hierarchical nanochannel systems have not yet achieved ion selectivity comparable to that of their counterparts. The many elaborately constructed hierarchical nanochannel systems are still accompanied by some limitations, for instance, complicated fabrication procedures and poor long-term robustness. In addition, it remains a challenge to systematically investigate the mechanism of ion

transport in terms of selectivity and transport flux. The contribution of each type of channel remains difficult to adequately and unambiguously reveal. Moreover, from the perspective of potential applications, although great progress has been made, many difficult issues remain to be resolved. For example, concentration polarization effects of the charged hierarchical nanochannel membrane reduced the difference in salt solution on both sides of the membrane and thus further decreased the osmotic energy conversion efficiency<sup>97</sup>. For separation, selectivity and separation are generally a pair of contradictions. Many reported studies have considered the enhancement in separation selectivity to the target of interest but have ignored the separation flux, which determines the separation efficiency to a great extent.

There is no doubt that the development of hierarchical nanochannels is in its mid-term stage. A variety of new nanochannel materials are continually emerging, and their potentials in multiple fields are presented. For instance, hierarchical nanochannel systems with sub-nanoscale ion channels have recently emerged and achieved extraordinary performance in selective ion transport. In addition to the currently reported MOFs and porous molecular crystal materials, various other types of framework materials with fine channels can also be expected to be used to construct hierarchical sub-nanochannel systems with different sizes and surface properties, which may result in super performance in ion transport. At the same time, the potential of hierarchically engineered nanochannels in many application areas is promising. In the future, their application in osmotic energy conversion may exhibit much higher efficiency. On the other hand, hierarchical nanochannel-based biosensors might result in increased access to higher quality diagnostic systems. Of particular note is that current hybrid nanopore systems can provide new engineering modifications to current proteins or solid-state nanopores so that they possess suitable pore sizes or functional groups to sense analytes. For example, a protein nanopore can be engineered through various chemical modifications to improve the affinity. Similarly, solid-state nanopores can also be modified with functional elements to construct hybrid hierarchical nanopores to sense small biomolecules. Undoubtedly, the focused research activities and broad prospects will advance the development of hierarchically engineered nanochannels to a new level of maturity.

### Acknowledgements

This work was supported by the National Natural Science Foundation of China (21922411, 22004120, and 22104013), National Key Research and Development Program of China (Grant No. 2022YFC3400800), Natural Science Foundation of Jiangxi Province (20212BAB213002), DICI Innovation Funding (DICI-RC201801, DICI I202008), Project funded by China Postdoctoral Science Foundation (2020M670799), and Liaoning Revitalization Talents Program (XLYC1802109).

### Author contributions

M.L., Y.X., and G.Q. conceived and designed the topic of this review article. M.L., Y.C., and Y.X. reviewed the literature and wrote the manuscript. M.L. and Y.X. prepared the figures. G.Q. reviewed and revised the writing. All authors read and approved the final manuscript.

### Competing interests

The authors declare no competing interests.

### Publisher's note

Springer Nature remains neutral with regard to jurisdictional claims in published maps and institutional affiliations.

Received: 16 August 2022 Revised: 11 November 2022 Accepted: 15 November 2022.

Published online: 31 March 2023

### References

- Gouaux, E. & Mackinnon, R. Principles of selective ion transport in channels and pumps. *Science* **310**, 1461–1465 (2005).
- Morais-Cabral, J. H., Zhou, Y. & MacKinnon, R. Energetic optimization of ion conduction rate by the K<sup>+</sup> selectivity filter. *Nature* **414**, 37–42 (2001).
- Doyle, D. A. et al. The structure of the potassium channel: molecular basis of K<sup>+</sup> conduction and selectivity. *Science* **280**, 69–77 (1998).
- Zhang, H. C., Tian, Y. & Jiang, L. Fundamental studies and practical applications of bio-inspired smart solid-state nanopores and nanochannels. *Nano Today* **11**, 61–81 (2016).
- Perez Sirkin, Y. A., Tagliazucchi, M. & Szeleifer, I. Transport in nanopores and nanochannels: some fundamental challenges and nature-inspired solutions. *Mater. Today Adv.* **5**, 100047 (2020).
- Zhang, Z., Wen, L. & Jiang, L. Bioinspired smart asymmetric nanochannel membranes. *Chem. Soc. Rev.* **47**, 322–356 (2018).
- Long, Z. et al. Recent advances in solid nanopore/channel analysis. *Anal. Chem.* **90**, 577–588 (2018).
- Sun, M. H. et al. Applications of hierarchically structured porous materials from energy storage and conversion, catalysis, photocatalysis, adsorption, separation, and sensing to biomedicine. *Chem. Soc. Rev.* **45**, 3479–3563 (2016).
- Kubo, Y. & Murata, Y. Control of rectification and permeation by two distinct sites after the second transmembrane region in Kir2.1 K<sup>+</sup> channel. *J. Physiol.* **531**, 645–660 (2001).
- Lu, J. et al. Ultrafast rectifying counter-directional transport of proton and metal ions in metal-organic framework-based nanochannels. *Sci. Adv.* **8**, eabl5070 (2022).
- Xu, W. et al. Recent advances in chiral discrimination on host-guest functionalized interfaces. *Chem. Commun.* **57**, 7480–7492 (2021).
- Li, X. et al. Role of outer surface probes for regulating ion gating of nanochannels. *Nat. Commun.* **9**, 40 (2018).
- Zhang, Z. et al. Bioinspired heterogeneous ion pump membranes: unidirectional selective pumping and controllable gating properties stemming from asymmetric ionic group distribution. *J. Am. Chem. Soc.* **140**, 1083–1090 (2018).
- Zhang, Z. et al. A bioinspired multifunctional heterogeneous membrane with ultrahigh ionic rectification and highly efficient selective ionic gating. *Adv. Mater.* **28**, 144–150 (2016).
- Esfandiari, A. et al. Size effect in ion transport through angstrom-scale slits. *Science* **358**, 511–513 (2017).
- Feng, J. et al. Observation of ionic coulomb blockade in nanopores. *Nat. Mater.* **15**, 850–855 (2016).
- Zhou, X. et al. Intrapore energy barriers govern ion transport and selectivity of desalination membranes. *Sci. Adv.* **6**, eabd9045 (2020).
- Guo, Y., Ying, Y., Mao, Y., Peng, X. & Chen, B. Polystyrene sulfonate threaded through a metal-organic framework membrane for fast and selective lithium-ion separation. *Angew. Chem. Int. Ed.* **55**, 15120–15124 (2016).
- Li, X. et al. Fast and selective fluoride ion conduction in sub-1-nanometer metal-organic framework channels. *Nat. Commun.* **10**, 2490 (2019).
- Mo, R. et al. In situ growth of ultrasmall nanochannels in porous anodized aluminum membrane and applied in detection of lead ion. *Anal. Chem.* **91**, 8184–8191 (2019).
- Tan, S. et al. Metal-organic framework-based micropipette is a metal ion responsive nanochannel after adsorbing H<sub>2</sub>S. *Chem. Commun.* **57**, 7152–7155 (2021).
- Xin, W. et al. Biomimetic KcsA channels with ultra-selective K<sup>+</sup> transport for monovalent ion sieving. *Nat. Commun.* **13**, 1701 (2022).
- Lu, J. et al. Efficient metal ion sieving in rectifying subnanochannels enabled by metal-organic frameworks. *Nat. Mater.* **19**, 767–774 (2020).
- Zhang, H., Li, X., Hou, J., Jiang, L. & Wang, H. Angstrom-scale ion channels towards single-ion selectivity. *Chem. Soc. Rev.* **51**, 2224–2254 (2022).
- Zhang, Z. et al. Ultrathin and ion-selective janus membranes for high-performance osmotic energy conversion. *J. Am. Chem. Soc.* **139**, 8905–8914 (2017).
- Zhu, X. et al. Unique ion rectification in hypersaline environment: a high-performance and sustainable power generator system. *Sci. Adv.* **4**, eaau1665 (2018).
- Sun, Y. et al. Tailoring a poly(ether sulfone) bipolar membrane: osmotic-energy generator with high power density. *Angew. Chem. Int. Ed.* **59**, 17423–17428 (2020).
- Xu, Y. L., Song, Y. J. & Xu, F. Tempo oxidized cellulose nanofibers-based heterogeneous membrane employed for concentration-gradient-driven energy harvesting. *Nano Energy* **79**, 105468 (2021).
- Xin, W. et al. High-performance silk-based membranes employed for osmotic energy conversion. *Nat. Commun.* **10**, 3876 (2019).
- Zhou, S. et al. Interfacial super-assembly of ordered mesoporous silica-alumina heterostructure membranes with pH-sensitive properties for osmotic energy harvesting. *ACS Appl. Mater. Interfaces* **13**, 8782–8793 (2021).
- Zhou, S. et al. Interfacial super-assembly of ordered mesoporous carbon-silica/AAO hybrid membrane with enhanced permselectivity for temperature- and pH-sensitive smart ion transport. *Angew. Chem. Int. Ed.* **60**, 26167–26176 (2021).
- Huang, Y. et al. Super-assembled chiral mesostructured heteromembranes for smart and sensitive couple-accelerated enantioseparation. *J. Am. Chem. Soc.* **144**, 13794–13805 (2022).
- Wang, C. et al. Fabrication of bio-inspired 2D MOFs/PAA hybrid membrane for asymmetric ion transport. *Adv. Funct. Mater.* **30**, 1908804 (2019).
- Xu, T. et al. Highly cation permselective metal-organic framework membranes with leaf-like morphology. *ChemSusChem* **12**, 2593–2597 (2019).
- Wang, W. et al. Carbon nanofibers membrane bridged with graphene nanosheet and hyperbranched polymer for high-performance osmotic energy harvesting. *Nano Res* <https://doi.org/10.1007/s12274-022-4634-6> (2022).
- Acar, E. T., Buchsbaum, S. F., Combs, C., Fornasiero, F. & Siwy, Z. S. Biomimetic potassium-selective nanopores. *Sci. Adv.* **5**, eaav2568 (2019).
- Xin, P. et al. Artificial K<sup>+</sup> channels formed by pillararene-cyclodextrin hybrid molecules: tuning cation selectivity and generating membrane potential. *Angew. Chem. Int. Ed.* **58**, 2779–2784 (2019).
- Lang, C. et al. Highly selective artificial potassium ion channels constructed from pore-containing helical oligomers. *Angew. Chem. Int. Ed.* **56**, 12668–12671 (2017).
- Ye, T. et al. Artificial sodium-selective ionic device based on crown-ether crystals with subnanometer pores. *Nat. Commun.* **12**, 5231 (2021).
- Li, X. et al. Unidirectional and selective proton transport in artificial heterostructured nanochannels with nano-to-subnano confined water clusters. *Adv. Mater.* **32**, e2001777 (2020).
- Tan, R. et al. Hydrophilic microporous membranes for selective ion separation and flow-battery energy storage. *Nat. Mater.* **19**, 195–202 (2020).
- Guo, Y. et al. A DNA-threaded ZIF-8 membrane with high proton conductivity and low methanol permeability. *Adv. Mater.* **30**, 1705155 (2018).
- Zhang, H. et al. Ultrafast selective transport of alkali metal ions in metal organic frameworks with subnanometer pores. *Sci. Adv.* **4**, eaag0066 (2018).
- Sheng, F. et al. Efficient ion sieving in covalent organic framework membranes with sub-2-nanometer channels. *Adv. Mater.* **33**, e2104404 (2021).
- Chen, L. et al. Unidirectional ion transport in nanoporous carbon membranes with a hierarchical pore architecture. *Nat. Commun.* **12**, 4650 (2021).
- Sui, X. et al. Engineered nanochannel membranes with diode-like behavior for energy conversion over a wide pH range. *ACS Appl. Mater. Interfaces* **11**, 23815–23821 (2019).
- Li, R., Jiang, J., Liu, Q., Xie, Z. & Zhai, J. Hybrid nanochannel membrane based on polymer/mof for high-performance salinity gradient power generation. *Nano Energy* **53**, 643–649 (2018).
- Yao, L., Li, Q., Pan, S., Cheng, J. & Liu, X. Bio-inspired salinity-gradient power generation with UIO-66-NH<sub>2</sub> metal-organic framework based composite membrane. *Front. Bioeng. Biotechnol.* **10**, 901507 (2022).

49. Liu, Y.-C., Yeh, L.-H., Zheng, M.-J. & Wu, K. C. W. Highly selective and high-performance osmotic power generators in subnanochannel membranes enabled by metal-organic frameworks. *Sci. Adv.* **7**, eabe9924 (2021).
50. Zhang, L. et al. Interfacial super-assembly of T-mode janus porous heterochannels from layered graphene and aluminum oxide array for smart oriented ion transportation. *Small* **17**, e2100141 (2021).
51. Huang, X. D. et al. Engineered PES/SPES nanochannel membrane for salinity gradient power generation. *Nano Energy* **59**, 354–362 (2019).
52. Hao, J. et al. Concise and efficient asymmetric homogeneous janus membrane for high-performance osmotic energy conversion based on oppositely charged montmorillonite. *Electrochim. Acta* **423**, 140581 (2022).
53. Hao, J., Yang, T., He, X., Tang, H. & Sui, X. Hierarchical nanochannels based on rod-coil block copolymer for ion transport and energy conversion. *Giant* **5**, 100049 (2021).
54. Zhang, Z. et al. Improved osmotic energy conversion in heterogeneous membrane boosted by three-dimensional hydrogel interface. *Nat. Commun.* **11**, 875 (2020).
55. Zhao, Y. et al. Robust sulfonated poly(ether ether ketone) nanochannels for high-performance osmotic energy conversion. *Natl. Sci. Rev.* **7**, 1349–1359 (2020).
56. Zhao, X. L. et al. Metal organic framework enhanced SPEEK/SPSF heterogeneous membrane for ion transport and energy conversion. *Nano Energy* **81**, 105657 (2021).
57. Li, C. et al. Large-scale, robust mushroom-shaped nanochannel array membrane for ultrahigh osmotic energy conversion. *Sci. Adv.* **7**, eabg2183 (2021).
58. Liu, X. et al. Power generation by reverse electrodialysis in a single-layer nanoporous membrane made from core-rim polycyclic aromatic hydrocarbons. *Nat. Nanotechnol.* **15**, 307–312 (2020).
59. Yang, J. et al. Advancing osmotic power generation by covalent organic framework monolayer. *Nat. Nanotechnol.* **17**, 622–628 (2022).
60. Hong, S. et al. Two-dimensional  $Ti_3C_2T_x$  MXene membranes as nanofluidic osmotic power generators. *ACS Nano* **13**, 8917–8925 (2019).
61. Ji, J. et al. Osmotic power generation with positively and negatively charged 2D nanofluidic membrane pairs. *Adv. Funct. Mater.* **27**, 1603623 (2017).
62. Xiao, K., Giusto, P., Wen, L., Jiang, L. & Antonietti, M. Nanofluidic ion transport and energy conversion through ultrathin free-standing polymeric carbon nitride membranes. *Angew. Chem. Int. Ed.* **57**, 10123–10126 (2018).
63. Qin, S. et al. High and stable ionic conductivity in 2D nanofluidic ion channels between boron nitride layers. *J. Am. Chem. Soc.* **139**, 6314–6320 (2017).
64. Zhang, Z. et al. Mechanically strong MXene/Kevlar nanofiber composite membranes as high-performance nanofluidic osmotic power generators. *Nat. Commun.* **10**, 2920 (2019).
65. Chen, C. et al. Bio-inspired nanocomposite membranes for osmotic energy harvesting. *Joule* **4**, 247–261 (2020).
66. Chen, C. et al. Bioinspired ultrastrong nanocomposite membranes for salinity gradient energy harvesting from organic solutions. *Adv. Energy Mater.* **10**, 1904098 (2020).
67. Xin, W. et al. Biomimetic nacre-like silk-crosslinked membranes for osmotic energy harvesting. *ACS Nano* **14**, 9701–9710 (2020).
68. Zhou, P., Yao, L., Chen, K. & Su, B. Silica nanochannel membranes for electrochemical analysis and molecular sieving: a comprehensive review. *Crit. Rev. Anal. Chem.* **50**, 424–444 (2020).
69. Lu, Y., Zhang, H., Zhu, Y., Marriott, P. J. & Wang, H. Emerging homochiral porous materials for enantiomer separation. *Adv. Funct. Mater.* **31**, 2101335 (2021).
70. Li, M. et al. Biomimetic calcium-inactivated ion/molecular channel. *Chem. Commun.* **57**, 7914–7917 (2021).
71. Laucirica, G. et al. Biomimetic solid-state nanochannels for chemical and biological sensing applications. *TrAC, Trends Anal. Chem.* **144**, 116425 (2021).
72. Welch, E. C., Powell, J. M., Clevinger, T. B., Fairman, A. E. & Shukla, A. Advances in biosensors and diagnostic technologies using nanostructures and nanomaterials. *Adv. Funct. Mater.* **31**, 2104126 (2021).
73. Chan, J. Y. et al. Incorporation of homochirality into a zeolitic imidazolate framework membrane for efficient chiral separation. *Angew. Chem. Int. Ed.* **57**, 17130–17134 (2018).
74. Lu, Y. et al. Homochiral MOF-polymer mixed matrix membranes for efficient separation of chiral molecules. *Angew. Chem. Int. Ed.* **58**, 16928–16935 (2019).
75. Chen, Y., Xia, L., Lu, Z., Li, G. & Hu, Y. In situ fabrication of chiral covalent triazine frameworks membranes for enantiomer separation. *J. Chromatogr. A* **1654**, 462475 (2021).
76. Zhang, C., Wu, B.-H., Ma, M.-Q., Wang, Z. & Xu, Z.-K. Ultrathin metal/covalent-organic framework membranes towards ultimate separation. *Chem. Soc. Rev.* **48**, 3811–3841 (2019).
77. Yuan, C. et al. Nanochannels of covalent organic frameworks for chiral selective transmembrane transport of amino acids. *J. Am. Chem. Soc.* **141**, 20187–20197 (2019).
78. Zhang, S., Zhou, J. & Li, H. Chiral covalent organic framework packed nanochannel membrane for enantioseparation. *Angew. Chem. Int. Ed.* **61**, e202204012 (2022).
79. Cheng, M. et al. Chiral nanochannels of ordered mesoporous silica constructed by a pillar[5]arene-based host-guest system. *ACS Appl. Mater. Interfaces* **13**, 27305–27312 (2021).
80. Li, M. et al. Biomimetic nanochannels for the discrimination of sialylated glycans via a tug-of-war between glycan binding and polymer shrinkage. *Chem. Sci.* **11**, 748–756 (2019).
81. Li, M. et al. Functional nanochannels for sensing tyrosine phosphorylation. *J. Am. Chem. Soc.* **142**, 16324–16333 (2020).
82. Xiong, Y. et al. Discerning tyrosine phosphorylation from multiple phosphorylations using a nanofluidic logic platform. *Anal. Chem.* **93**, 16113–16122 (2021).
83. Ali, M., Neumann, R. & Ensinger, W. Sequence-specific recognition of DNA oligomer using peptide nucleic acid (PNA)-modified synthetic ion channels: PNA/DNA hybridization in nanoconfined environment. *ACS Nano* **4**, 7267–7274 (2010).
84. Zhang, F., Sun, Y., Tian, D. & Li, H. Chiral selective transport of proteins by cysteine-enantiomer-modified nanopores. *Angew. Chem. Int. Ed.* **56**, 7186–7190 (2017).
85. Ding, D., Gao, P., Ma, Q., Wang, D. & Xia, F. Biomolecule-functionalized solid-state ion nanochannels/nanopores: features and techniques. *Small* **15**, 1804878 (2019).
86. Ma, Q. et al. Functional solid-state nanochannels for biochemical sensing. *TrAC, Trends Anal. Chem.* **115**, 174–186 (2019).
87. Zhao, X.-P. et al. Nanochannel-ion channel hybrid device for ultrasensitive monitoring of biomolecular recognition events. *Anal. Chem.* **91**, 1185–1193 (2019).
88. Chu, Z. et al. A separation-sensing membrane performing precise real-time serum analysis during blood drawing. *Angew. Chem. Int. Ed.* **59**, 18701–18708 (2020).
89. Xue, L. et al. Solid-state nanopore sensors. *Nat. Rev. Mater.* **5**, 931–951 (2020).
90. Shi, W., Friedman, A. K. & Baker, L. A. Nanopore sensing. *Anal. Chem.* **89**, 157–188 (2017).
91. Zhang, S. et al. Bottom-up fabrication of a proteasome–nanopore that unravels and processes single proteins. *Nat. Chem.* **13**, 1192–1199 (2021).
92. Hall, A. R. et al. Hybrid pore formation by directed insertion of  $\alpha$ -haemolysin into solid-state nanopores. *Nat. Nanotechnol.* **5**, 874–877 (2010).
93. Engst, C. R. et al. DNA origami nanopores. *Nano Lett.* **12**, 512–517 (2012).
94. Gu, L.-Q., Braha, O., Conlan, S., Cheley, S. & Bayley, H. Stochastic sensing of organic analytes by a pore-forming protein containing a molecular adapter. *Nature* **398**, 686–690 (1999).
95. Su, Z., Wei, Y. & Kang, X.-F. Simultaneous high-resolution detection of bioenergetic molecules using biomimetic-receptor nanopore. *Anal. Chem.* **91**, 15255–15259 (2019).
96. Bétermier, F. et al. Single-sulfur atom discrimination of polysulfides with a protein nanopore for improved batteries. *Commun. Mater.* **1**, 59 (2020).
97. Wang, L., Wang, Z., Patel, S. K., Lin, S. & Elimelech, M. Nanopore-based power generation from salinity gradient: why it is not viable. *ACS Nano* **15**, 4093–4107 (2021).
98. Lu, J. et al. Ultrasensitive monovalent metal ion conduction in a three-dimensional sub-1 nm nanofluidic device constructed by metal-organic frameworks. *ACS Nano* **15**, 1240–1249 (2021).